Lower land use emissions increased net land carbon sink during warming hiatus period

Shilong Piao[1,2,3], Zhuo Liu[1], Mengtian Huang[1], Xuhui Wang[1,4], Philippe Ciais[4], Josep G. Canadell[5], Kai Wang[1], Ana Bastos[4], Pierre Friedlingstein[6], Richard A. Houghton[7], Corinne Le Quéré[8], Yongwen Liu[1], Ranga B. Myneni[9], Shushi Peng[1], Julia Pongratz[10], Stephen Sitch[11], Tao Yan[1], Yilong Wang[4], Tao Wang[2,3], Zaichun Zhu[1], Donghai Wu[1]

[1] Sino-French Institute for Earth System Science, College of Urban and Environmental Sciences, Peking University, Beijing 100871, China

[2] Key Laboratory of Alpine Ecology and Biodiversity, Institute of Tibetan Plateau Research, Chinese Academy of Sciences, Beijing 100085, China

[3] Center for Excellence in Tibetan Earth Science, Chinese Academy of Sciences, Beijing 100085, China

[4] Laboratoire des Sciences du Climat et de l'Environnement, CEA CNRS UVSQ, Gif-sur-Yvette 91191, France

[5] Carbon Project, CSIRO Oceans and Atmosphere, Canberra, Australian Capital Territory 2601, Australia

[6] College of Engineering, Mathematics and Physical Sciences, University of Exeter, North Park Road, Exeter EX4 4QF, UK

[7] Woods Hole Research Center, 149 Woods Hole Road, Falmouth, Massachusetts 02540, USA

[8] Tyndall Centre for Climate Change Research, University of East Anglia, Norwich Research Park, Norwich, NR4 7TJ, UK

[9] Department of Earth and Environment, Boston University, Boston, Massachusetts 02215, USA

[10] Max Planck Institute for Meteorology, Bundesstraße 53, 20146 Hamburg, Germany

[11] College of Life and Environmental Sciences, University of Exeter, North Park Road, Exeter

EX4 4RJ, UK

The terrestrial carbon sink has shown an acceleration after 1998, coincident with the warming hiatus[1,2]. However, different mechanisms were proposed[1,2]. Here we analyse recent change in the net land carbon sink (NLS) and its driving factors using atmospheric inversions results[3,4] and terrestrial carbon models. We show that the linear trend of NLS during 1998-2012 (0.17±0.05 PgC yr^{-2}) is three times larger than during 1980-1998 (0.05±0.05 PgC yr^{-2}). This NLS intensification cannot be explained by CO_2 fertilization (0.02±0.11 PgC yr^{-2}) and climate change (-0.03±0.15 PgC yr^{-2}) according to terrestrial model simulation[5,6]. Thus, we looked more into the contribution of changes in land use emissions (E_{LUC}) estimated from the bookkeeping model of Houghton et al.[7] showing decreasing E_{LUC} as the dominant driver (73%) of the intensification of NLS during 1998-2012. This reduction of land-use change emissions is due to both decreased tropical forest area loss and increased afforestation in northern temperate regions. Calculating E_{LUC} with the inversion-based estimate shows consistently reduced E_{LUC}, while another bookkeeping model[8] did not reproduce such change probably due to missing the signal of reduced tropical deforestation. These results highlight the importance of better constraining emissions from land use change to understand recent trends in land carbon sinks.

47 Coincident with the warming hiatus of 1998-2012[9-11], the vegetation greening trend
48 observed from several satellite products stalled after 1998 in most regions[12-16] while the global
49 land carbon sink has continued to increase[1,2]. Keenan et al.[1] and Ballantyne et al.[2] analysed
50 this signal from the residual terrestrial carbon sink (RLS) calculated by difference between
51 emissions from fossil fuel and land use, and ocean uptake and atmospheric CO_2 growth rate.
52 The mechanisms behind the recent increase in RLS were inconsistent between the two studies.
53 Keenan et al.[1] suggest increasing photosynthesis and decreased respiration, whereas
54 Ballantyne et al.[2] suggest decreasing photosynthesis and thus reduced respiration being the
55 only mechanism through which RLS increased during the hiatus. Furthermore, the seasonal
56 and spatial patterns of changes in land carbon sink do not match with those of temperature
57 changes[17]. Of note is the fact that systematic errors in land use emissions [7] directly transfer as
58 bias of RLS[5,18]. Thus, instead of RLS, we revisit changes in the net land carbon sink (NLS)
59 including land use emissions and its driving factors using atmospheric inversions and land
60 carbon models.

61 The NLS estimated from the two inversions (see Methods) and from the global CO_2
62 budget[19] show a three-times faster increase after 1998 (0.17±0.05 PgC yr^{-2}, mean ± 1 standard
63 error) than in the decade before (0.05±0.05 PgC yr^{-2}) (Fig. 1 and Supplementary Table 1, see
64 Methods). The limit of 1998 is the one used by IPCC[20] and previous carbon cycle study[21] as
65 the beginning of the hiatus, but using 2001 or 2002 as the starting year of the warming hiatus
66 yields similar results (Supplementary Table 2). The enlarging positive trend in NLS after 1998
67 (i.e. NLS intensification) is also found on a 5-years moving window (Supplementary Fig. 1)
68 and in different inversion versions with more atmospheric CO_2 measurement sites but for
69 shorter period (Supplementary Table 3 and Fig. 2).

70 NLS can be decomposed as the sum of three components, net primary productivity
71 (NPP), heterotrophic respiration and fires in natural ecosystems (HR+F) and net carbon

emissions from land use change (E_{LUC}). The fraction of fire emissions that happens during land use change, known as deforestation fires, is included in E_{LUC}, while carbon emission from fossil fuels for land management is not included in E_{LUC}. To explain why NLS increased faster after 1998, we consider three mechanisms: (M1) NPP increased faster than before, forcing a sink intensification; (M2) heterotrophic respiration and fires (HR+F) increased at a slower rate than before or declined, consistent with slower warming rates; (M3) E_{LUC} emissions decreased[22].

Trends in NPP For the first mechanism, we analysed NPP changes over the past 30 years using the dynamic vegetation models (DGVM) from the TRENDY project and satellite observation-based NPP from Smith et al.[12] (hereafter SM16, see Methods). As shown in Figure 1B and 1D, both satellite-derived NPP and modelled NPP showed significant positive trends (an indication of enhanced carbon assimilation) before 1998 (SM16: 0.12±0.03 PgC yr^{-2}, $P < 0.01$; DGVMs mean: 0.15±0.04 PgC yr^{-2}, $P < 0.01$). After 1998, however, the satellite-based NPP shows a significantly ($P<0.05$) smaller positive trend (0.04 ± 0.04 PgC yr^{-2}, $P > 0.05$) than before. By comparison, four of the eight DGVMs do not show deceleration of NPP (i.e. reduced trend of NPP) after 1998, with trend change of NPP ranging from -0.08±0.05 PgC yr^{-2} ($P < 0.05$) to 0.11±0.06 PgC yr^{-2} ($P < 0.01$) (Supplementary Fig. 3). On average, the DGVMs show almost no change of NPP trend (-0.001±0.067 PgC yr^{-2}, $P > 0.1$) between the period before 1998 and that after 1998 (Fig. 2), and can thus barely explain (<1%) the intensification of NLS after 1998. A recent commentary[23] suggested that the disagreement of NPP trends between SM16 and DGVM is likely due to the underestimate of the CO_2 fertilization effect on satellite-based NPP. However, continued increase of CO_2 concentration over past three decades may not explain the intensification of NLS after 1998. The leaf area index (LAI) derived from GIMMS satellite products stalled in the recent period 1998-2012, which is not captured by DGVMs (Supplementary Fig. 4). This overestimate of

the LAI trend in the period after 1998 suggests that DGVMs may under-estimate the deceleration of NPP in the recent decade captured in SM16. Therefore, the forcing from NPP change alone cannot explain why NLS intensified.

Trends in HR and natural fire To analyse the second mechanism (M2) we analysed changes in HR based on the same DGVM results[5,6]. As shown in Fig. 2 and Supplementary Table 1, a reduction in the positive trend of HR (i.e. a deceleration of carbon emission from HR) in simulations where models were driven by changing CO_2 and climate was found by most DGVMs, with six out of the eight models showing a reduced trend of HR after 1998 ranging from -0.06±0.03 PgC yr^{-2} ($P < 0.01$) to 0.06±0.08 PgC yr^{-2} ($P > 0.05$). The small deceleration of HR (-0.01±0.04 PgC yr^{-2}, $P > 0.05$), however, accounts for less than 9% (-47% - 49%) of the observed intensification of NLS. According to factorial DGVM simulations, the effect of climate change alone (see Methods) did cause a significant deceleration of HR in the period 1998-2012 (-0.04±0.05 PgC yr^{-1}, $P > 0.05$) compared to the period 1980-1998 (Fig. 2), consistent with a slower warming rate between 1998 and 2012. However, the climate driven HR deceleration (i.e. deceleration in carbon emission) is also paralleled by a NPP deceleration (i.e. deceleration in carbon uptake) due to climate change alone in the DGVM models (-0.06±0.10 PgC yr^{-2}, $P > 0.05$; Fig. 2). This indicates that the NLS intensification during 1998-2012 cannot be attributed to climate change alone in the DGVM models. The simulation results of these models further show that rising atmospheric CO_2 can only explain 19% of the NLS intensification (Fig. 2), and that the combinations of CO_2 and climate change cancel each other. These results suggest that mechanisms other than CO_2 fertilization and climate change are responsible for the observed intensification of the NLS.

Besides HR, a reduction in natural fire emission could be another cause the intensification in the NLS. Accounting natural fires at global scale remains challenging, because satellite-based burn area cannot readily distinguish natural fires from other causes[24,25].

Therefore, we analysed trends in fire simulated by four TRENDYv2 DGVMs, which considered wild fire processes. The models exhibited large differences in the change of fire emissions trend during the two periods (CLM4.5: -0.052±0.020 PgC yr^{-1}, $P < 0.01$; LPJ: 0.004±0.009 PgC yr^{-1}, $P > 0.05$; VISIT: 0.007±0.018 PgC yr^{-1}, $P > 0.05$; LPJ-GUESS: 0.013±0.024 PgC yr^{-1}, $P > 0.05$) (Supplementary Fig. 5). However, even considering the full model range of trend estimates, the natural fire emission probably contributes negatively to intensification of NLS (-6%±25%).

Trends in net carbon emission from land use change Over the last thirty years there has been a slow-down of forest losses[26-30]. According to the latest Forest Resources Assessment (FRA 2015) by Food and Agriculture Organization of the United Nations[31], the annual rate of net forest loss decreased from 7.27 M ha yr^{-1} in the 1990s to 3.99 M ha yr^{-1} in the 2000s, primarily owing to less logging in tropical regions and increased plantations in northern temperate lands (Supplementary Table 4 and Fig. 6). Therefore, the NLS intensification can also reflect decreased E_{LUC} during 1998-2012.

We estimated E_{LUC} using the latest version of the bookkeeping model from Houghton et al.[7] (hereafter BK), which was widely used and adopted by the Global Carbon Project in accounting annual global carbon budget[32]. The global E_{LUC} is a source of 1.13 PgC yr^{-1}, which is found mostly in tropical regions (1.31 PgC yr^{-1}), primarily Southeast Asia (0.54 PgC yr^{-1}), South America (0.38 PgC yr^{-1}) and Africa (0.38 PgC yr^{-1}) (Supplementary Fig. 7a). Tropical regions are found to be the largest contributor to global E_{LUC} emissions, followed by the Southern Hemisphere temperate regions as a slight source (1% of global E_{LUC}) (Supplementary Fig. 7a). We then compared the linear trend of E_{LUC} over the globe between 1980-1998 and 1998-2012. The deceleration of E_{LUC} contributes to a trend change of 0.09±0.01 PgC yr^{-2} ($P < 0.01$) (Fig. 3), explaining 73% of NLS intensification. This result suggests that the faster increase of NLS after 1998 is primarily explained by decreasing E_{LUC}.

As shown in Fig. 3, the deceleration in global E_{LUC} between 1980-1998 and 1998-2012 is attributed to tropical regions, where a decline of -0.08±0.01 PgC yr^{-2} ($P < 0.01$) in E_{LUC} trend is found (about 92% of the total decrease in global E_{LUC} trend). The decline was largely in Southeast Asia (-0.05±0.01 PgC yr^{-2}, $P < 0.01$) and South America (-0.016±0.004 PgC yr^{-2}, $P < 0.01$) (Fig. 3), where the annual rate of net forest loss declined during the 2000s compared with 1990s[31]. For example, the rate of net forest loss in South America decreased from 4 M ha yr^{-1} during the 1990s to 3.87 M ha yr^{-1} during the 2000s, whereas the net loss rate in Southeast Asia during the 2000s (0.64 M ha yr^{-1}) was only 30% of that during the 1990s (2.11 M ha yr^{-1}) (Supplementary Fig. 6 and Table 4). For NH temperate regions, E_{LUC} was found to decelerate between the two periods, with a linear trend of -0.010±0.001 PgC yr^{-2} after 1998 ($P < 0.01$; about 11% of the total decrease in global E_{LUC} trend). Temperate North America accounted for the largest fraction (89%; -0.009±0.006 PgC yr^{-2}, $P < 0.01$) of decreasing E_{LUC} in the northern temperate zone, mainly due to the fact that the forest area decrease of -0.35 M ha yr^{-1} in the 1990s was reversed to an increase of 0.22 M ha yr^{-1} after 2000[31] (Supplementary Fig. 6 and Table 4).

In addition to BK based on FAO/FRA land use areas and regional carbon response curves to land use change[18], we also explored E_{LUC} estimates with two other methods, which are the bookkeeping model of Hansis et al.[8] (hereafter BKH) based on Land Use Harmonization (LUH) data from 1500 to 2004[33] and the Global Carbon Project update from 2005 to 2012[5] (see Methods), and E_{LUC} estimated by forming the difference between the net land-atmosphere CO_2 flux from atmospheric inversions and the fraction of this flux attributed to natural ecosystems simulated under the TRENDY S2 DGVM simulation (hereafter $E_{Inversion\text{-}LF\text{-}DGVMs(S2)}$, see Methods). Globally, the change in trend of global E_{LUC} after 1998 by $E_{Inversion\text{-}LF\text{-}DGVMs(S2)}$ (-0.07±0.05 PgC yr^{-2}, $P < 0.05$) was similar to that by BK, but BKH estimated little change in trend of E_{LUC} (-0.01±0.01 PgC yr^{-2}, $P > 0.05$) for the same period.

The lack of trend change by BKH may come from uncertainties in land cover input dataset. Important differences between the land use input used in BK, which is directly based on FAO/FRA, and the harmonized land use dataset by Hurtt et al.[33] used in BKH are assumptions on shifting cultivation in the tropics and additional assumptions introduced in the latter dataset to make the country-level FAO/FRA data spatially explicit. Forest cover changes are not explicitly indicated by the harmonized land use dataset but deduced from changes in agricultural areas and thus can differ largely from forest inventory data both in magnitude and in trends (Supplementary Fig. 8). For example, The BKH estimated E_{LUC} over South America exhibited positive change (0.007±0.008 PgC yr^{-2}, $P > 0.05$) during the warming hiatus period, which is in contrast to forest survey data suggesting a reduced rate of deforestation in 2000s[31]. The shift of land cover dataset in 2004 is also a potential issue making BKH more uncertain in estimating change in E_{LUC} trend during the recent decade. The general consensus between BK and $E_{Inversion\text{-}LF\text{-}DGVMs(S2)}$ in estimating change of E_{LUC} trend globally and over South America suggests the potential of utilizing this new method in estimating E_{LUC}. However, it also differs from BK in estimating trend change of E_{LUC} at regional scale, for example, over Africa (-0.002±0.001 PgC yr^{-2}, $P < 0.05$ by BK vs. 0.04±0.03 PgC yr^{-2}, $P < 0.05$ by $E_{Inversion\text{-}LF\text{-}DGVMs(S2)}$; Supplementary Fig. 7b). The lack of atmospheric CO_2 observations over Africa can be a large source of uncertainties in atmospheric inversion, as indicated by the large error bars in regional E_{LUC} estimates (Supplementary Fig. 7b). The uncertainties in land carbon models[6] are also propagated in $E_{Inversion\text{-}LF\text{-}DGVMs(S2)}$.

In summary, our results confirm an intensification in the NLS during the warming hiatus, (1998-2012) as compared to the preceding period (1980-1998). Using different approaches, we found that a number of drivers were responsible for the enhanced rate of the NLS. The decreasing trend in net carbon emissions from land use change was the dominant cause during warming hiatus period. The decreasing emissions from land use change were not driven by a

lower rate of warming during this period, but by reduced deforestation in the tropics and increased afforestation in NH temperate regions. Consistent with Keenan et al.[1], we found a lower positive trend of HR due to a lower rate of warming during the second period. But contrary to them, our analysis, based on an ensemble of DGVMs under different scenarios instead of a semi-empirical model[1], shows little effect of HR trends on the NLS, mainly because of the compensating effects of CO_2 fertilization (increasing carbon emissions from HR through higher input) and climate change (decreasing carbon emissions from HR). Note that large uncertainties still remain with estimates of carbon flux from land use change and its trend over the last thirty years, particularly in East Asia, South America, Africa and Europe. Reducing this uncertainty is a top priority for future work to more accurately predict the future evolution of the global carbon cycle and its feedback to climate change. To this end, detailed information on LULCC transitions[28,34] with high spatio-temporal resolution, and on carbon response functions to these transitions[30,35] is needed. In addition, various forms of land use management (e.g. wood harvest, shifting cultivation, cropland management, fire management, peatland drainage) are often inconsistently and incompletely represented in DGVMs[5,18]. A better characterization of these critical processes is required in future studies.

Methods

Satellite-based NDVI and NPP data. The Normalized Difference Vegetation Index (NDVI), which has been widely used to monitor vegetation activity, was obtained from Global Inventory Modelling and Mapping Studies (GIMMS) third-generation product ($NDVI_{3g}$) at a resolution of 8 km×8 km from 1982 to 2015[36].

The satellite-derived net primary productivity (NPP) was from MODIS[13] and a recent study by Smith et al.[12] (SM16). For the latter, NPP was calculated based on MODIS NPP algorithm[13], but driven by 30-year (1982-2011) GIMMS fraction of photosynthetically active radiation (FPAR) and leaf area index (LAI) data[12]. Further details about satellite-derived NPP data can be found in Smith et al.[12] and Zhao & Running[13]. Note that the MODIS results only cover the period from 2001 onwards. Therefore, we only included the MODIS results in Supplementary Fig. 9 to show that the stall of NPP during warming hiatus period is not an artifact from the only one long-term satellite-derived net primary productivity (NPP) data from Smith et al.[12].

Dynamic global vegetation models (DGVMs). An ensemble of eight dynamic global vegetation models (Supplementary Table 5 from the project "Trends and drivers of the regional scale sources and sinks of carbon dioxide" (TRENDY) were used to simulate the carbon balance of terrestrial ecosystems during the period 1980-2012. These models provided outputs of Net Biome Productivity (NBP), Net Primary Productivity (NPP) and Heterotrophic Respiration (HR). Here we used NBP to reflect the magnitude of net land carbon sink (NLS, NLS = NBP = NPP - HR - D, D refers to other losses of carbon due to disturbance, including carbon emissions from land use change). Note that we adopted the convention that a sink of CO_2 is defined as positive (removing CO_2 from the atmosphere).

The DGVMs were coordinated to perform three simulations (S1, S2 and S3) following the TRENDY protocol[6]. In simulation S1, only atmospheric CO_2 concentration was varied. In

simulation S2, atmospheric CO_2 and climate were varied. In simulation S3, atmospheric CO_2, climate and land use were varied. The effects of rising atmospheric CO_2, climate change and land use change on NLS can then be obtained from S1, the difference between S2 and S1, and the difference between S3 and S2, respectively. All models used the same forcing datasets, of which global atmospheric CO_2 concentration was from the combination of ice core records and atmospheric observations[37]; historical climate fields were from CRU-NCEP dataset (http://dods.extra.cea.fr/data/p529viov/cruncep/); land use data were from the Land Use Harmonization dataset[31] based on the History Database of the Global Environment (HYDE)[38]. All the model outputs were resampled to a spatial resolution of $0.5^o \times 0.5^o$ based on the nearest neighbour method.

Note that there is a large difference between TRENDYv2 and TRENDYv4 in the estimate of NLS trend before and after 1998 under S3 simulation (Supplementary Fig. 10). On average, NLS in TRENDYv2 shows a non-significant trend before 1998 and a significant increasing trend after 1998 (Supplementary Fig. 10h), which is consistent with the results from the global carbon budget and atmospheric inversions. However, in TRENDYv4, an opposite case was found (Supplementary Fig. 10h). This difference between TRENDYv2 and TRENDyv4 in simulating the observed NLS trend mainly results from the simulation of land use change rather than S2 simulation (Supplementary Fig. 10h). This not only indicates large uncertainties in the simulation of land use change (Supplementary Fig. 7), but suggests the potential effect of land use change on NLS trend. Although TRENDYv4 used an updated and improved input of land use change maps (HYDE3.2)[39] compared with TRENDYv2 (HYDE3.1), we did not adopt it to estimate carbon emissions from land use change given that it did not capture the trend of NLS before and after 1998. Overall, we only used TRENDY results derived from S1 and S2 simulation in our main text, and proposed a new way to estimate land use change emission by combining the results from atmospheric inversions and TRENDY models under

S2 simulation (see below).

Global carbon budget. To gain a better understanding of the net land carbon sink, we also used data from global carbon budget coordinated by the Global Carbon Project (GCP)[19]. Here the net land sink was inferred as a residual of fossil fuel emissions, atmospheric CO_2 accumulation and ocean sink, which is independent from atmospheric inversions.

Atmospheric CO_2 inversion data. Atmospheric CO_2 inversions offer a method in which CO_2 observation networks, transport models and a prior knowledge of fluxes are utilized to estimate net land-atmosphere carbon exchange[40]. This top-down approach allows us to compare the magnitude of net land carbon sink (NLS) with that from bottom-up method based on DGVMs. Given our long-term study period from 1980 to 2012, here we used two inversion products: MACC_v15 from Chevallier et al.[3] (hereafter MACC, available time period: 1979-2015) and JENA_S81_v3.8 from Rödenbeck et al.[4] (hereafter JENA, available time period: 1981-2014). The original spatial resolution of MACC and JENA is 1.875°latitude×3.75°longitude and 3.75°latitude×5°longitude, respectively.

It should be noted that there are differences between these two inversions in number of observation sites as constraint, transport models and prior flux information[40]. As recommended in previous studies[40,41], a standard fossil fuel and cement production flux (FFC) should be subtracted from the total posterior fluxes when comparing net land flux from different CO_2 inversions. This is due to the fact that differences in prior FFC will manifest as differences in the estimated natural flux[38]. Thus, here we took the fossil fuel flux which is used in GCP carbon budget as a standard and subtracted it from the total posterior fluxes for both CO_2 inversions to obtain the "fossil corrected" NLS, although the global fossil fuel emissions are quite consistent between the two inversions and with the GCP data (Supplementary Fig. 11). Note that the FFC data used in GCP carbon budget was from the Carbon Dioxide Information Analysis Center (CDIAC,

289 http://cdiac.ornl.gov/trends/emis/meth_reg.html) and energy statistics published by BP
290 (http://www.bp.com/en/global/corporate/about-bp.html).

291 **Net carbon flux from land use change (E_{LUC}).** We used the estimates by Houghton et al.[7]
292 (hereafter BK) for carbon fluxes due to land use change. In this method, ground-based
293 measurements of carbon density are combined with land cover change data from the Forest
294 Resource Assessment (FRA) of the Food and Agriculture Organization (FAO) using a
295 semi-empirical bookkeeping model, in which standard growth and decomposition curves are
296 used to track changes in carbon pools[18]. Using the estimate by Houghton et al.[7] is consistent
297 with the global carbon budget estimates provided by the Global Carbon Project[42], but may
298 conceal large uncertainties associated with land use change itself as well as LUC-related
299 carbon fluxes. We therefore include in the supplemental analyses two additional approaches:
300 The second approach is also a bookkeeping method but from Hansis et al.[8] (hereafter BKH).
301 Although BKH largely follows the bookkeeping method developed by Houghton et al.[43,44],
302 there are key differences between BKH and BK: BKH is spatially explicit at a resolution of
303 $0.5^{o}\times0.5^{o}$[8], whereas BK is constructed based on aggregated, non-spatial national and
304 international statistics[18]; BKH used Land Use Harmonization dataset from 1500 to 2004[31] and
305 the Global Carbon Project update from 2005 to 2012 as input[8] while BK used FAO/FRA land
306 use change data[18]; other differences between BKH and BK are the accounting of successive
307 LULCC events including their interactions in BKH and different assumptions on the
308 allocation of agricultural land on natural vegetation[8]. Note that the data available now from
309 Houghton et al.[43,44] and Hansis et al.[8] does not enable us to obtain the quantifiable
310 uncertainties for trends.

311 Apart from above two bookkeeping approaches, here we developed a new way to
312 indirectly estimate E_{LUC} using the difference of land carbon flux from atmospheric inversions,
313 the flux from lateral transport (LF) and that from DGVMs under S2 simulation (driven by

rising CO_2 and climate change, not taking into account LF) (hereafter referred to $E_{Inversion\text{-}LF\text{-}DGVMs(S2)}$). This approach was based on the assumption that the effect of changing atmospheric CO_2 concentration and climate are well modelled by DGVMs so that the difference between inversion fluxes (including all CO_2 sources and components), lateral carbon flux and DGVM modelled fluxes under S2 simulation equals the net source from land use and land management.

The processes of lateral carbon transport generally involve (1) the trade of food and wood products; (2) carbon export from land to ocean by rivers. In terms of the lateral carbon flux associated with food and wood trade (Supplementary Fig. 12), we first derive the annual import and export data of food and wood products from FAO statistical databases (http://www.fao.org/faostat/en/#data). Then the food and wood data are converted into dry biomass and into carbon using specific conversion factors. For food products, we adopted crop-specific coefficients (including dry matter content of harvested biomass and carbon content of harvested dry matter, see Supplementary Table 6) following Wolf et al.[45] and Kyle et al.[46]. For wood products, we adopted an average wood density of 0.5 and 0.45 carbon concentration in dry biomass following Ciais et al.[47]. In terms of the carbon exported from ecosystems by rivers, we included dissolved organic carbon (DOC), particulate organic carbon (POC) and dissolved inorganic carbon (DIC) from 45 major zones (MARCATS: MARgins and CATchments Segmentation) and 149 sub-units (COSCATs: Coastal Segmentation and related CATchments)[48,49] (http://www.biogeomod.net/geomaps/, see Supplementary Table 7). Then we aggregated the riverine carbon transport into continental scale (Supplementary Fig. 13). However, it should be noted that the carbon transport data is only a rough estimate and lack temporal evolution. Besides, it is unclear whether the exported carbon by rivers is from old deposits or from current photosynthesis. In addition, time series of the carbon exports from rivers are not available. Therefore, we did not count this part in the

calculation of LF.

Note that we obtained eighteen estimates from $F_{Inversion\text{-}LF\text{-}DGVMs(S2)}$ approach, as eight DGVMs and two atmospheric inversions were considered in the analysis. All datasets from atmospheric inversions and DGVMs were first regridded into a common 0.5°×0.5° grid using nearest neighbor interpolation method. We also performed the same analyses by regridding all the datasets into a common 1°×1° or 2°×2° grid, and found similar results (Supplementary Fig. 14). In addition, given that BK was based on national data and not spatially explicit, we obtained latitudinal results (the bottom left in Fig. 3) by roughly aggregating northern North America, Europe and Asian Russia into boreal region, southern North America, West/Central/South Asia and East Asia to Northern Hemisphere (NH) temperate region, South America, Africa and Southeast Asia to tropics, and Oceania to Southern Hemisphere (SH) temperate region.

There is a S3 simulation of TRENDY where DGVMs are driven by the land cover dataset (LUH) in addition to change in climate and atmospheric CO_2. Thus, the difference of S3 and S2 simulations may also represent the model simulated emission of land use change. However, comparing the difference between S3 and S2 and E_{LUC} estimated by the bookkeeping or inversion-based approach are difficult, because DGVMs do not simulate the full range of processes related to E_{LUC} (not all DGVMs account for example for wood and crop harvest or shifting cultivation[42]). Further, land use change emissions derived as difference between S3 and S2 differ in the terms that are included as compared to other approaches[48]. Most notably, the loss of additional sink capacity is attributed to E_{LUC} using S3 minus S2, while it is excluded from E_{LUC} derived from bookkeeping models or the inversion-based approach. Lastly, the input land cover dataset has discontinuity issue in the recent decade and different models also have different assumption converting LUH dataset into model-specific land cover inputs, making it less reliable in estimating trend in the recent

decade. Therefore, we do not include the difference of S3 and S2 simulation by DGVMs in this study.

Statistical analysis. We calculated the trend of NLS, NPP, HR, NDVI and E_{LUC} during three study periods (1980-2012, 1980-1998, and 1998-2012) based on Linear Least Square Regression analysis, in which above five indicators were regarded as dependent variables and year as independent variable. The slope of the regression was then defined as the trend. The standard error of linear regression coefficient (slope) was defined as the uncertainty of the linear trend. Note that for the average trend of different data sources, the uncertainty of its trend was estimated as the root-mean-square of the standard error of for each data sources under the assumption that data from different datasets is independent from each other. Based on this, we obtained the change of above five indicators' trend between the second period (1998-2012) and the first period (1980-1998). The dividing year 1998 is selected according to IPCC description of the warming hiatus period[20]. However, the intensification of NLS and dominant contribution of E_{LUC} will not change, if trend analyses starts from 2001/2002 after the El Nino/La Nina events at the end of 20th century (Supplementary Table 2). Note that here changes in the intensity of each component of NLS were indicated by changes in the magnitude (absolute value) of each term. In this case, a positive trend in NPP / HR, F and E_{LUC} refers to an increase of carbon assimilation / carbon emission, and vice versa, a negative trend in NPP / HR, F and E_{LUC} indicates a decline in carbon assimilation / carbon emission. The statistics of the change in trend for each flux was estimated using bootstrap analyses[51]. We first obtained probability distribution of NLS trend before and after 1998 in 500-time bootstrapping. Then the probability distribution in the change in trend for each flux was calculated based on the differences of trends among the sampling of the two probability distributions. For clarification, NLS intensification indicates increase in the trend of NLS after 1998. Similarly, acceleration/deceleration of a flux (NPP, HR, fire and E_{LUC}) indicates

larger/smaller trend of the flux during 1998-2012 than that during 1980s-1998.

Data availability. The GIMMS $NDVI_{3g}$ datasets are available at http://ecocast.arc.nasa.gov/data/pub/gimms/3g.v0/. The satellite-derived NPP dataset is available on request from W. K. Smith[12]. The MODIS NPP dataset is available on request from M. Zhao[13]. Net carbon flux from land use change (E_{LUC}) estimated using the bookkeeping approach is available on request from R. A. Houghton[7] and E. Hansis[8], respectively. Model outputs generated by Dynamic Global Vegetation Model (DGVM) groups are available from Stephen Stich (s.a.sitch@exeter.ac.uk) or Pierre Friedlingstein (p.friedlingstein@exeter.ac.uk) upon request.

400 **Reference**

401 1. Keenan, T. F. *et al.* Recent pause in the growth rate of atmospheric CO2 due to enhanced
402 terrestrial carbon uptake. *Nat Commun* **7**, 13428 (2016).

403 2. Ballantyne, A. *et al.* Accelerating net terrestrial carbon uptake during the warming hiatus
404 due to reduced respiration. *Nat. Clim. Change* **7**, 148-152 (2017).

405 3. Chevallier, F. *et al*. CO2 surface fluxes at grid point scale estimated from a global 21 year
406 reanalysis of atmospheric measurements. *J. Geophys. Res.* **115**, D21307,
407 doi:10.1029/2010JD013887 (2010).

408 4. Rödenbeck, C. Estimating CO_2 sources and sinks from atmospheric mixing ratio
409 measurements using a global inversion of atmospheric transport, Technical Report 6, Max
410 Planck Institute for Biogeochemistry, Jena, available at:
411 http://www.bgc-jena.mpg.de/uploads/Publications/TechnicalReports/tech_report6.pdf, 2005.

412 5. Le Quéré, C. *et al.* Global carbon budget 2013. *Earth Syst. Sci. Data* **6**, 235-263 (2014).

413 6. Sitch, S. *et al*. Recent trends and drivers of regional sources and sinks of carbon dioxide.
414 *Biogeosciences* **12**, 653–679 (2015).

415 7. Houghton, R. A. & Nassikas, A. A. Global and regional fluxes of carbon from land use
416 and land cover change 1850–2015. *Glob. Biogeochem. Cycles* **31**,
417 doi:10.1002/2016GB005546 (2017).

418 8. Hansis, E., Davis, S. J. & Pongratz, J. Relevance of methodological choices for
419 accounting of land use change carbon fluxes. *Glob. Biogeochem. Cycles* **29**, 1230-1246
420 (2015).

421 9. Easterling, D. R. & Wehner, M. F. Is the climate warming or cooling? *Geophys. Res. Lett.*
422 **36**, L08706, doi:10.1029/2009GL037810 (2009).

10. Kaufmann, R. K., Kauppi, H., Mann, M. L. & Stock, J. H. Reconciling anthropogenic climate change with observed temperature 1998-2008. *Proc. Natl Acad. Sci. USA*. **108**, 11790-11793 (2011).

11. Cohen, J. L., Furtado, J. C., Barlow, M. & Alexeev, V. A. Asymmetric seasonal temperature trends. *Geophys. Res. Lett.* **39**, L04705, doi:10.1029/2011GL050582 (2012).

12. Smith, W. K. *et al*. Large divergence of satellite and Earth system model estimates of global terrestrial CO_2 fertilization. *Nat. Clim. Change* **6**, 306-310 (2016).

13. Zhao, M. & Running, S. W. Drought-induced reduction in global terrestrial net primary production from 2000 through 2009. *Science* **329**, 940-943 (2010).

14. Jong, R., Verbesselt, J., Schaepman, M. E. & Bruin, S. Trend changes in global greening and browning: contribution of short-term trends to longer-term change. *Glob. Change Biol.* **18**, 642-655 (2012).

15. Mohammat, A. *et al*. Drought and spring cooling induced recent decrease in vegetation growth in Inner Asia. *Agric. For. Meteorol.* **178**: 21-30 (2013).

16. Kong, D., Zhang, Q., Singh, V. P. & Shi, P. Seasonal vegetation response to climate change in the Northern Hemisphere (1982–2013). *Glob. Planet. Change* **148**, 1-8 (2017).

17. Zhu, Z. *et al*. The accelerating land carbon uptake of the 2000s may not be driven predominantly by the warming hiatus. *Geophys Res Lett.* **45**: 1402-1409 (2018).

18. Houghton, R. A. *et al*. Carbon emissions from land use and land-cover change. *Biogeosciences* **9**, 5125-5142 (2012).

19. Le Quéré, C. *et al.* Global carbon budget 2015. *Earth Syst. Sci. Data* **7**, 349-396 (2015).

20. Hartmann, D. L. et al. Observations: Atmosphere and Surface. in Climate Change 2013: The Physical Science Basis (eds Stocker, T. F. et al.) 192–194 (Cambridge Univ. Press, Cambridge, 2013).

21. Ballantyne, A. *et al.* Accelerating net terrestrial carbon uptake during the warming hiatus

448 due to reduced respiration. *Nature Climate Change* **7**, 148-152 (2017).
449 22. Grassi, G. *et al*. The key role of forests in meeting climate targets requires science for
450 credible mitigation. *Nat. Clim. Change* **7**, 220-226 (2017).
451 23. De Kauwe, M. G. *et al*. Satellite based estimates underestimate the effect of CO_2
452 fertilization on net primary productivity. *Nat. Clim. Change* **6**, 892-893 (2016).
453 24. Giglio, L., Randerson, J. T. & van der Werf, G. R. Analysis of daily, monthly, and annual
454 burned area using the fourth-generation global fire emissions database (GFED4). *J. Geophys.*
455 *Res. Biogeosci.* **118**, 317-328 (2013).
456 25. Andela, N. *et al.* A human-driven decline in global burned area. *Science* **356**, 1356-1362
457 (2017).
458 26. Rudel, T. K. *et al.* Forest transitions: towards a global understanding of land use change.
459 *Glob Environ Change* **15**, 23-31 (2005).
460 27. Sánchezcuervo, A. M., Aide, T. M., Clark, M. L. & Etter, A. Land Cover Change in
461 Colombia: Surprising Forest Recovery Trends between 2001 and 2010. *PLoS One* **7**, e43943
462 (2012).
463 28. Magliocca, N. R. *et al.* Synthesis in land change science: methodological patterns,
464 challenges, and guidelines. *Reg Environ Change* **15**, 211-226 (2015).
465 29. Chazdon, R. L. *et al.* Carbon sequestration potential of second-growth forest regeneration
466 in the Latin American tropics. *Sci Adv* **2**, doi: 10.1126/sciadv.1501639 (2016).
467 30. Poorter, L. *et al.* Biomass resilience of Neotropical secondary forests. *Nature* **530**, 211
468 (2016).
469 31. Food and Agriculture Organization of the United States (FAO). Global Forest Resources
470 Assessment 2015: How are the world's forests changing?
471 http://www.fao.org/forest-resources-assessment/en/ (2015).
472 32. Le Quéré, C. *et al.* Global carbon budget 2014. *Earth Syst Sci Data* **7**, 47-85 (2015).

473 33. Hurtt, G. C. *et al*. Harmonization of land-use scenarios for the period 1500-2100: 600
474 years of global gridded annual land-use transitions, wood harvest, and resulting secondary
475 lands. *Climatic change* **109**, 117-161 (2011).
476 34. Erb, K. H. *et al.* Bias in the attribution of forest carbon sinks. *Nat. Clim. Change* **3**,
477 854-856 (2013).
478 35. Poeplau, C. *et al.* Temporal dynamics of soil organic carbon after land-use change in the
479 temperate zone-carbon response functions as a model approach. *Glob. Change Biol.* **17**,
480 2415-2427 (2011).
481 36. Tucker, C. J. *et al.* An extended AVHRR 8-km NDVI dataset compatible with MODIS
482 and SPOT vegetation NDVI data. *Int. J. Remote Sens.* **26**, 4485–4498 (2005).
483 37. Keeling, C. D. & Whorf, T. P. Atmospheric carbon dioxide record from Mauna Loa.
484 Trends: A Compendium of Data on Global Change. Carbon Dioxide Information Analysis
485 Center, Oak Ridge National Laboratory, Oak Ridge, TN (2005).
486 38. Klein Goldewijk, K., Beusen, A., Van Drecht, G. & De Vos, Martine. The HYDE 3.1
487 spatially explicit database of human-induced global land-use change over the past 12,000
488 years. *Global Ecol. Biogeogr.* **20**, 73-86 (2011).
489 39. Klein Goldewijk, K. A historical land use data set for the Holocene; HYDE 3.2. *EGU*
490 *General Assembly Conference Abstracts* **18**, 1574 (2016).
491 40. Peylin, P. *et al.* Global atmospheric carbon budget: results from an ensemble of
492 atmospheric CO_2 inversions. *Biogeosciences* **10**, 6699-6720 (2013).
493 41. Thompson, R. L. *et al.* Top–down assessment of the Asian carbon budget since the mid
494 1990s. *Nat. Commun.* **7**, DOI: 10.1038/ncomms10724 (2016).
495 42. Le Quéré, C. *et al.* Global carbon budget 2016. *Earth Syst Sci Data* **8**, 605 (2016).
496 43. Houghton, R. A. *et al*. Changes in the Carbon Content of Terrestrial Biota and Soils
497 between 1860 and 1980: A Net Release of CO_2 to the Atmosphere. *Ecological monographs*

53, 235-262 (1983).

44. Houghton, R. A. Revised estimates of the annual net flux of carbon to the atmosphere from changes in land use and land management 1850–2000. *Tellus B* **55**, 378-390 (2003).

45. Wolf, J. *et al*. Biogenic carbon fluxes from global agricultural production and consumption. *Glob. Biogeochem. Cycles* **29**, 1617-1639 (2015).

46. Kyle, P. et al. GCAM 3.0 agriculture and land use: data sources and methods. Pacific Northwest National Laboratory. PNNL-21025 (2011).

47. Ciais, P. *et al*. The impact of lateral carbon fluxes on the European carbon balance. *Biogeosciences Discuss* **3**, 1529-1559 (2006).

48. Laruelle, G. G. *et al*. Global multi-scale segmentation of continental and coastal waters from the watersheds to the continental margins. *Hydrol. Earth Syst. Sc.* **17**, 2029 (2013).

49. Regnier, P. *et al*. Anthropogenic perturbation of the carbon fluxes from land to ocean. *Nature Geosci.* **6**, 597-607 (2013).

50. Pongratz, J., Reick, C. H., Houghton, R. & House, J. Terminology as a key uncertainty in net land use and land cover change carbon flux estimates. *Earth System Dynamics* **5**, 177 (2014).

51. Manly B. F. J. Randomization, bootstrap and Monte Carlo methods in biology (CRC Press, 2006).

Acknowledgements

This study was supported by the National Natural Science Foundation of China (41530528), the 111 Project (B14001), and the National Youth Top-notch Talent Support Program in China. We thank the TRENDY modelling group for providing the model simulation data.

Author Contributions

S.Piao designed the study. Z.L performed the analysis. S.Piao and Z.L drafted the paper. All authors contributed to the interpretation of the results and to the text.

Author Information

The authors declare no competing financial interests. Correspondence and requests for materials should be addressed to S.Piao (slpiao@pku.edu.cn).

Figure legends

Figure 1 Anomalies and liner trends of global annual net land carbon sink (NLS) (a, c) and net primary productivity (NPP) (b, d). Our whole study period is from 1980 to 2012, and we calculated the trends of above variables for three time periods: 1980-2012, 1980-1998 and 1998-2012. In the left panels, positive value refers to a net carbon sink, while negative value refers to a net carbon source. The shaded area in the left panels indicates data uncertainty (±1σ). In the right panel, we denote significant trends ($P < 0.05$) with two asterisk based on t test. The error bars in the right panels indicate the standard error of linear trend for each dataset. In panel (d), the range of the data (minimum-maximum range) across different models is given as colored vertical bars with the solid line showing the average value. Note that different colors correspond to different sources of data (see Methods), which are noted in the legends of each panel.

Figure 2 Change in the trend of net land carbon sink (NLS), net primary productivity (NPP) and heterotrophic respiration (HR) estimated by eight Dynamic Global Vegetation Models (DGVMs) under different scenarios between 1998-2012 and 1980-1998. For each model, the change in the trend of NLS / NPP / HR were obtained as the trend of each variable during 1998-2012 minus that during 1980-1998. Results for the effect of rising atmospheric CO_2 concentration ('CO_2'), climate change ('CLI'), and above two factors combined ('CO_2+CLI') are shown. On each box, the central line marks the median, the edges of the box correspond to the 25th and 75th percentiles, and the whiskers extend to the range of the data. The solid dot shows the average value of the model results.

Figure 3 Linear trend of net carbon emission from land use change (E_{LUC}) and change in E_{LUC} trend between 1998-2012 and 1980-1998. The bottom left show results at latitudinal scale, including boreal (50°N-90°N), northern temperate (23°N-50°N), tropical (23°N-23°S) and southern temperate region (23°S-60°S). The E_{LUC} trend during each of the two periods as

555 well as change in E_{LUC} trend between two periods are obtained based on annual E_{LUC} from the
556 bookkeeping method (BK, see Methods). A positive trend refers to increased E_{LUC} during
557 corresponding period, while a negative trend refers to decreased E_{LUC} during corresponding
558 period. The error bars indicate the uncertainty for E_{LUC} trend / the change in E_{LUC} trend. The
559 uncertainty of the linear trend was estimated as the standard error of linear regression
560 coefficient (slope), while the uncertainty of the change in E_{LUC} trend was estimated using
561 bootstrap analyses (see Methods).
562

Figure 1

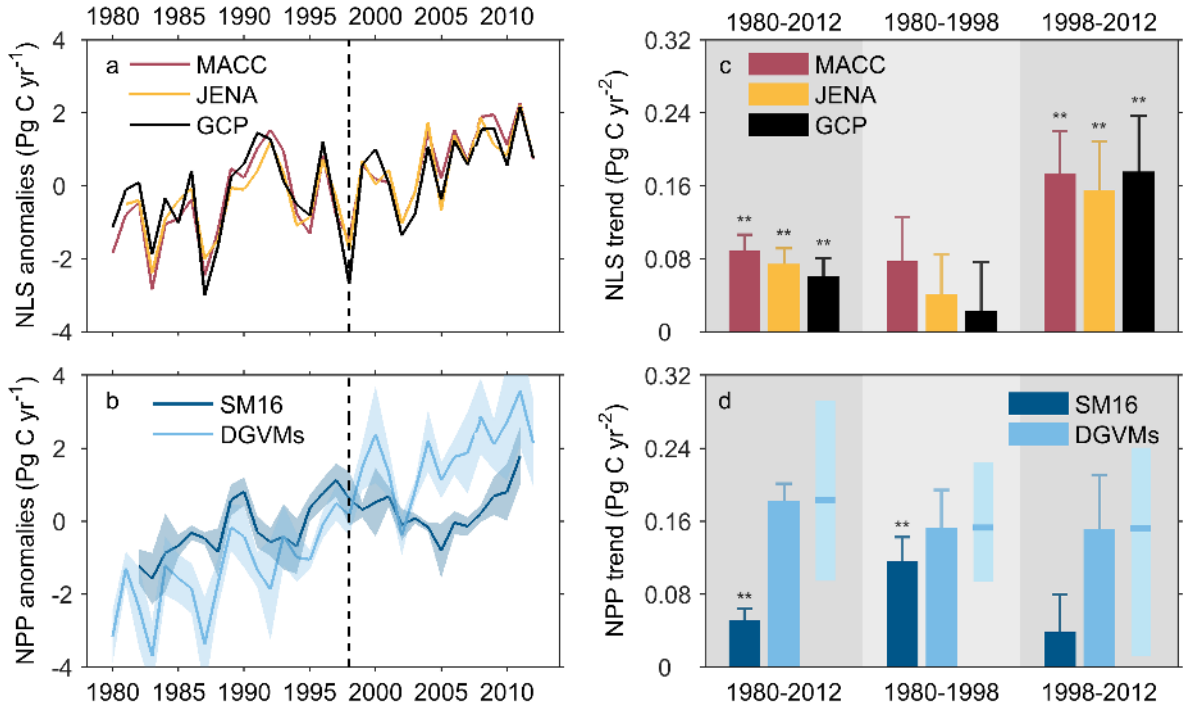
1980 1985 1990 1995 2000 2005 2010
a
MACC
JENA
GCP
NLS anomalies (Pg C yr-1)
b
SM16
DGVMs
NPP anomalies (Pg C yr-1)
1980-2012
1980-1998
1998-2012
c
NLS trend (Pg C yr-2)
d
NPP trend (Pg C yr-2)
**

567 **Figure 2**

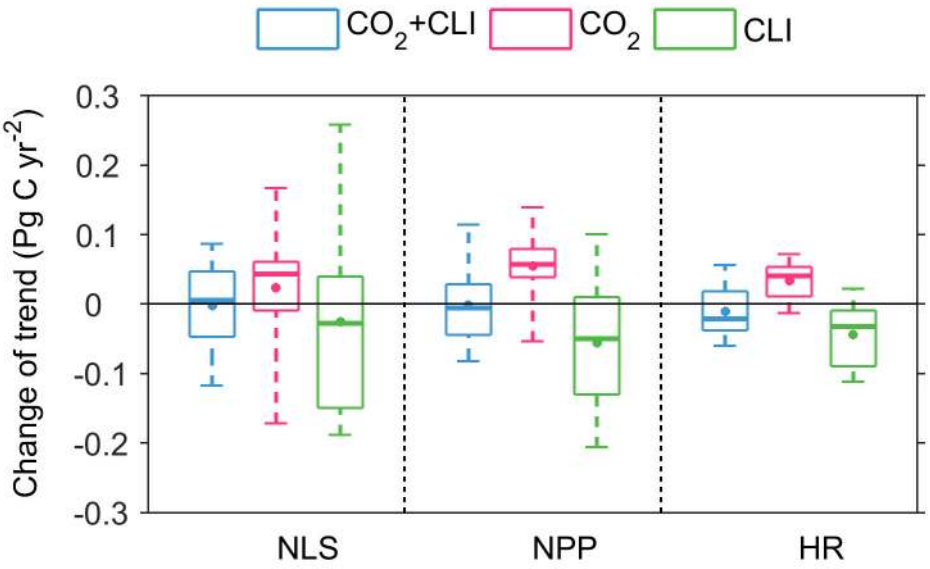

568

569

570 **Figure 3**

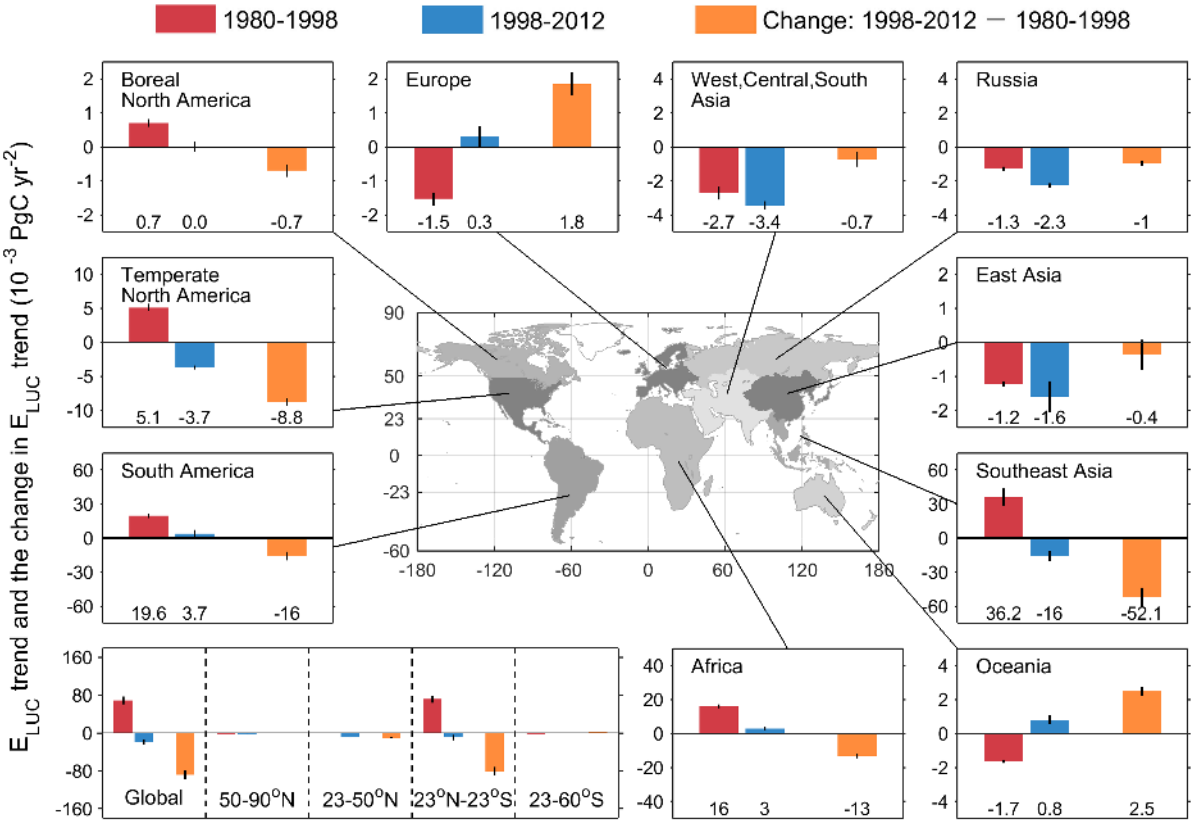

571

572